

# Counting solutions from finite samplings

Haiping Huang<sup>1,2</sup> and Haijun Zhou<sup>1</sup>

<sup>1</sup>*State Key Laboratory of Theoretical Physics, Institute of Theoretical Physics,  
Chinese Academy of Sciences, Beijing 100190, China*

<sup>2</sup>*Department of Physics, The Hong Kong University of Science and Technology, Hong Kong, China*

(Dated: July 18, 2018)

We formulate the solution counting problem within the framework of inverse Ising problem and use fast belief propagation equations to estimate the entropy whose value provides an estimate on the true one. We test this idea on both diluted models (random 2-SAT and 3-SAT problems) and fully-connected model (binary perceptron), and show that when the constraint density is small, this estimate can be very close to the true value. The information stored by the salamander retina under the natural movie stimuli can also be estimated and our result is consistent with that obtained by Monte Carlo method. Of particular significance is sizes of other metastable states for this real neuronal network are predicted.

PACS numbers: 84.35.+i, 02.50.Tt, 75.10.Nr, 89.70.Cf

## I. INTRODUCTION

Counting the number of solutions for random constraint satisfaction problems is a very important and nontrivial problem which belongs to #P-complete class in computational complexity [1] and is much harder than determining whether a random formula has any solutions. In practice, we can only sample a very small part of a huge solution space which contains an exponential number of solutions. However, can we predict the number of solutions in the whole solution space only based on a finite number of sampled solutions? This issue has generated broad interests across a variety of different disciplines such as computer science, probabilistic reasoning, statistical physics and computational biology [2–10]. An efficient sample-based counting strategy was proposed in Ref. [3]. This strategy successively sets the most balanced variable until an exact counter is feasible on the reduced formula, and provides a lower bound on the true count. Alternatively, we address the solution counting problem within the framework of inverse Ising problem in examples of diluted models—random  $K$ -SAT problems and fully-connected model—binary perceptron, and show that our method yields an estimate whose value could be very close to the true count when the constraint density is small. The constraint density is defined as the ratio of the number of constraints to that of variables in the system.

The inverse Ising problem [11] has recently attracted much attention not only in the development of fast mean field inverse algorithms [9, 12–14] but also in modeling vast amounts of biological data [7, 15–17]. The pairwise Ising model is able to capture most of the correlation structure of the real neuronal network activity and is much more informative than the independent model where each neuron is assumed to fire independently [7, 18]. The observed collective behavior of a large neuronal network results from interactions of many individual neurons. The joint activity patterns for a retina under naturalistic stimuli were reported to convey information about the visual stimuli [8, 19]. Estimating the information stored by the real neuronal network directly from data remains an open and important issue. We show in this work the information can be estimated reliably and sizes of metastable states for the neuronal network can also be predicted.

The paper is organized as follows. The inverse Ising problem is introduced in Sec. II, together with a brief description of the susceptibility propagation algorithm used to infer the disordered Ising model. In Sec. III, we present the belief propagation to estimate the entropy from the data and apply this method to predict the entropies of four different examples only from a limited number of samplings. Finally, the conclusion suggests some implications of our study as well as potential applications of the presented methodology.

## II. THE INVERSE ISING PROBLEM

For a system of  $N$  variables, one can collect  $P$  configurations or solutions  $\{\sigma_i^\nu\}(i = 1, \dots, N; \nu = 1, \dots, P)$  either from real biological experiments (e.g., spike trains in multi-electrode array recordings [7]) or from random walks in the solution space of a model. We assume  $\sigma_i$  takes Ising-type value  $\pm 1$ . The task of the inverse Ising problem is to find couplings  $\{J_{ij}\}$  and fields  $\{h_i\}$  to construct a minimal model

$$P_{\text{Ising}}(\boldsymbol{\sigma}) = \frac{1}{Z} \exp \left[ \sum_{i < j} J_{ij} \sigma_i \sigma_j + \sum_i h_i \sigma_i \right] \quad (1)$$

such that its magnetizations and pairwise correlations are compatible with those measured, i.e.,  $\langle \sigma_i \rangle_{\text{Ising}} = \langle \sigma_i \rangle_{\text{data}}$ ,  $\langle \sigma_i \sigma_j \rangle_{\text{Ising}} = \langle \sigma_i \sigma_j \rangle_{\text{data}}$ .  $Z$  is the partition function and the inverse temperature  $\beta = 1$  as it can be absorbed in the strength of couplings and fields. Hereafter, we define the measured magnetization and connected correlation as  $m_i \equiv \langle \sigma_i \rangle_{\text{data}}$  and  $C_{ij} \equiv \langle \sigma_i \sigma_j \rangle_{\text{data}} - m_i m_j$  respectively where  $\langle \cdots \rangle_{\text{data}}$  denotes the average over the sampled configurations or solutions.

We use susceptibility propagation (SusProp) to infer the couplings and fields. SusProp passes messages along the oriented edges of the network by iterative updating. To run SusProp, two kinds of messages are needed. One is the cavity magnetization of variable  $i$  in the absence of variable  $j$  denoted as  $m_{i \rightarrow j}$ ; the other is the cavity susceptibility  $g_{i \rightarrow j, k}$  that is the response of cavity field of variable  $i$  without variable  $j$  to a local perturbation of external field of variable  $k$  [12]. The update rule can be derived using belief propagation Eq. (4) and fluctuation-response relation [12, 20, 21] and reads as follows [21]:

$$m_{i \rightarrow j} = \frac{m_i - m_{j \rightarrow i} \tanh J_{ij}}{1 - m_i m_{j \rightarrow i} \tanh J_{ij}} \quad (2a)$$

$$g_{i \rightarrow j, k} = \delta_{ik} + \sum_{l \in \partial i \setminus j} \frac{1 - m_{l \rightarrow i}^2}{1 - (m_{l \rightarrow i} \tanh J_{li})^2} \tanh J_{li} g_{l \rightarrow i, k} \quad (2b)$$

$$J_{ij}^{\text{new}} = \frac{\epsilon}{2} \log \left( \frac{(1 + \tilde{C}_{ij})(1 - m_{i \rightarrow j} m_{j \rightarrow i})}{(1 - \tilde{C}_{ij})(1 + m_{i \rightarrow j} m_{j \rightarrow i})} \right) + (1 - \epsilon) J_{ij}^{\text{old}} \quad (2c)$$

$$\tilde{C}_{ij} = \frac{C_{ij} - (1 - m_i^2) g_{i \rightarrow j, j}}{g_{j \rightarrow i, j}} + m_i m_j \quad (2d)$$

where  $\partial i \setminus j$  denotes neighbors of variable  $i$  except  $j$ ,  $\delta_{ik}$  is the Kronecker delta function and  $\epsilon \in [0, 1]$  is introduced as a damping factor and should be appropriately chosen to prevent the absolute updated  $\tanh(J_{ij})$  from being larger than 1. In practice, all couplings are initially set to be zero and for every directed edge of the network, the message  $m_{i \rightarrow j}$  is randomly initialized in the interval  $[-1.0, 1.0]$  and  $g_{i \rightarrow j, k} = 0$  if  $i \neq k$  and 1.0 otherwise. The SusProp rule Eq. (2) is then iterated until either the inferred couplings converge within a predefined precision  $\eta^{(1)}$  or the preset maximal number of iterations  $\mathcal{T}_{\text{max}}^{(1)}$  is exceeded. After the set of couplings is obtained, the fields are inferred via  $h_i = \tanh^{-1}(m_i) - \sum_{l \in \partial i} \tanh^{-1}[\tanh J_{li} m_{l \rightarrow i}]$ .

To ensure a reliable estimate of the parameters, we define a convergence fraction  $R$  as the ratio of the number of converged couplings to the total number of edges in the network. In the non-convergent case, we take the inferred parameters corresponding to  $R_{\text{max}} = \max\{R_t, t = 1, \dots, \mathcal{T}_{\text{max}}^{(1)}\}$  where  $R_t$  is the convergence fraction of  $t$ -th iteration.  $R_{\text{max}} = 1.0$  if the update rule converges. For an inverse problem,  $\{m_i, C_{ij}\}$  serve as inputs to the update rule, and they are computed from  $P$  sampled solutions or configurations. We use stochastic local search algorithms to sample the solution space of random  $K$ -SAT ( $K = 2, 3$  here) formulas and that of the binary perceptron. For the retinal network, the configurations were obtained from the spike trains in the multi-electrode recording experiments (data courtesy of Gasper Tkacik, Refs. [7, 8]).

### III. ESTIMATING THE ENTROPY FROM THE DATA

We derive the entropy of the constructed Ising model Eq. (1) under Bethe approximation (also called cavity method [22]) assuming sufficiently weak interactions among variables. We compute the entropy through site contributions  $\Delta S_i$  and edge contributions  $\Delta S_{ij}$  as  $S_{\text{Ising}} = N s_{\text{Ising}} = \sum_i \Delta S_i - \sum_{\langle ij \rangle} \Delta S_{\langle ij \rangle}$ :

$$\begin{aligned}
\Delta S_i = & \log Z_i - \frac{1}{Z_i} \left[ h_i e^{h_i} \prod_{l \in \partial i} \cosh J_{li} (1 + \tanh J_{li} m_{l \rightarrow i}) - h_i e^{-h_i} \prod_{l \in \partial i} \cosh J_{li} (1 - \tanh J_{li} m_{l \rightarrow i}) \right. \\
& + e^{h_i} \sum_{l \in \partial i} \left[ J_{li} \sinh J_{li} (1 + \tanh J_{li} m_{l \rightarrow i}) + J_{li} \cosh J_{li} (1 - \tanh^2 J_{li}) m_{l \rightarrow i} \right] \cdot \prod_{j \in \partial i \setminus l} \cosh J_{ij} (1 + \tanh J_{ij} m_{j \rightarrow i}) \\
& \left. + e^{-h_i} \sum_{l \in \partial i} \left[ J_{li} \sinh J_{li} (1 - \tanh J_{li} m_{l \rightarrow i}) - J_{li} \cosh J_{li} (1 - \tanh^2 J_{li}) m_{l \rightarrow i} \right] \cdot \prod_{j \in \partial i \setminus l} \cosh J_{ij} (1 - \tanh J_{ij} m_{j \rightarrow i}) \right]
\end{aligned} \tag{3a}$$

$$\Delta S_{(ij)} = \log Z_{ij} - J_{ij} \frac{\tanh J_{ij} + m_{i \rightarrow j} m_{j \rightarrow i}}{1 + \tanh J_{ij} m_{i \rightarrow j} m_{j \rightarrow i}} \tag{3b}$$

where  $\partial i \setminus l$  denotes neighbors of variable  $i$  except  $l$ .  $Z_i = e^{h_i} \prod_{l \in \partial i} \cosh J_{li} (1 + \hat{m}_{l \rightarrow i}) + e^{-h_i} \prod_{l \in \partial i} \cosh J_{li} (1 - \hat{m}_{l \rightarrow i})$  and  $Z_{ij} = \cosh J_{ij} (1 + \tanh J_{ij} m_{i \rightarrow j} m_{j \rightarrow i})$ . The cavity magnetization  $m_{i \rightarrow j}$  obeys simple recursive equations:

$$m_{i \rightarrow j} = \frac{e^{h_i} \prod_{l \in \partial i \setminus j} (1 + \hat{m}_{l \rightarrow i}) - e^{-h_i} \prod_{l \in \partial i \setminus j} (1 - \hat{m}_{l \rightarrow i})}{e^{h_i} \prod_{l \in \partial i \setminus j} (1 + \hat{m}_{l \rightarrow i}) + e^{-h_i} \prod_{l \in \partial i \setminus j} (1 - \hat{m}_{l \rightarrow i})} \tag{4a}$$

$$\hat{m}_{l \rightarrow i} = \tanh J_{li} m_{l \rightarrow i} \tag{4b}$$

We first randomly initialize  $m_{i \rightarrow j} \in [-1.0, 1.0]$  for every directed edge of the reconstructed network, then iterate Eq. (4) until all messages converge within the precision  $\eta^{(2)}$  or the maximal number of iterations  $\mathcal{T}_{\max}^{(2)}$  is reached. From the fixed point, the entropy can be computed via Eq. (3). The case where some variable, say  $i$  is positively frozen, i.e., corresponding measured magnetization  $m_i = 1.0$ , can also be handled. In this case,  $h_i = +\infty$ , and  $\Delta S_i$  is reduced to be  $\log Z'_i - \frac{Z_i}{Z'_i}$  where  $Z'_i = \prod_{l \in \partial i} \cosh J_{li} (1 + \tanh J_{li} m_{l \rightarrow i})$  and  $Z''_i = \sum_{l \in \partial i} \left[ J_{li} \sinh J_{li} (1 + \tanh J_{li} m_{l \rightarrow i}) + J_{li} \cosh J_{li} (1 - \tanh^2 J_{li}) m_{l \rightarrow i} \right] \cdot \prod_{j \in \partial i \setminus l} \cosh J_{ij} (1 + \tanh J_{ij} m_{j \rightarrow i})$ . The edge contribution remains unchanged. The negatively frozen case is similarly treated. In numerical simulations, we adopt  $\mathcal{T}_{\max}^{(2)} = 500$ ,  $\eta^{(2)} = 10^{-4}$ ,  $\mathcal{T}_{\max}^{(1)} = 2000$ .  $\eta^{(1)}$  as well as  $\epsilon$  depends on the following specific applications.

We remark here that Eq. (3) is used specifically for the solution counting problem where we now have known the magnetizations and correlations and additionally some frozen cases (some  $m_i = +1$  or  $-1$ ) should be treated. On the other hand, the coupling or field distributions depend on the collected data and Eq. (3) is derived only under the weakly-coupled approximation but the fully connected topology is reserved. The first point is, the entropy we try to estimate is not only for two-body interaction system (e.g., random 2-SAT) but also for three-body interaction system and densely-interacted system (e.g., the binary perceptron where each constraint involves all variables of the system). The second point is, the sampled solutions come from the zero energy ground state and the sampling process is always confined in a single cluster (solutions in it are connected with each other by single variable flips).

All underlying parameters of pairwise Ising model are predicted directly from the observed data and the entropy of the original model is estimated based on the constructed Ising model. We emphasize here that two layers of approximations are made. The first one is the disordered Ising model Eq. (1) is used to approximate the original model. When estimating the entropy from the data, we actually do not know the original model. The second layer is we use mean-field methods, specifically the message passing algorithms to infer the underlying parameters of the pairwise Ising model. Since the computational complexity of SusProp is  $\mathcal{O}(N^3)$  for the fully-connected network, we focus on small size networks with  $N$  of order  $\mathcal{O}(10^2)$ . When the constraint density is small, the efficiency of our methodology is supported by two concrete examples: random  $K$ -SAT problem and the binary perceptron. For these two examples, we use  $s_{\text{true}}$  to represent the entropy density computed by belief propagation with the knowledge of the original model (for details, see Ref. [23] for random  $K$ -SAT problem and Ref. [24] for binary perceptron). To show the efficiency of the pairwise Ising model, we also compute the independent entropy  $S_{\text{ind}} = N s_{\text{ind}} = - \sum_i \left[ \frac{1+m_i}{2} \log \frac{1+m_i}{2} + \frac{1-m_i}{2} \log \frac{1-m_i}{2} \right]$  assuming  $P(\boldsymbol{\sigma}) \approx \prod_i P_i(\sigma_i)$ . For retinal network, we could neither know the true model underlying the network nor get the true value for the entropy (when the network is large). Therefore we just compare the result obtained by our current fast belief propagation with that obtained by time-consuming Monte Carlo method and show that the belief propagation not only reproduces the entropy value evaluated by Monte Carlo method but also yields rich information about the metastable states which are relevant for neuronal population coding [8, 19]. In this case, we denote  $s_{\text{BP}}$  as the entropy density estimated by belief propagation and  $s_{\text{MC}}$  estimated by Monte Carlo method. Note that both belief propagation and Monte Carlo method under the reconstructed Ising model yield approximate value for the true entropy since we consider only up to second-order correlations in the observed data while the system may develop

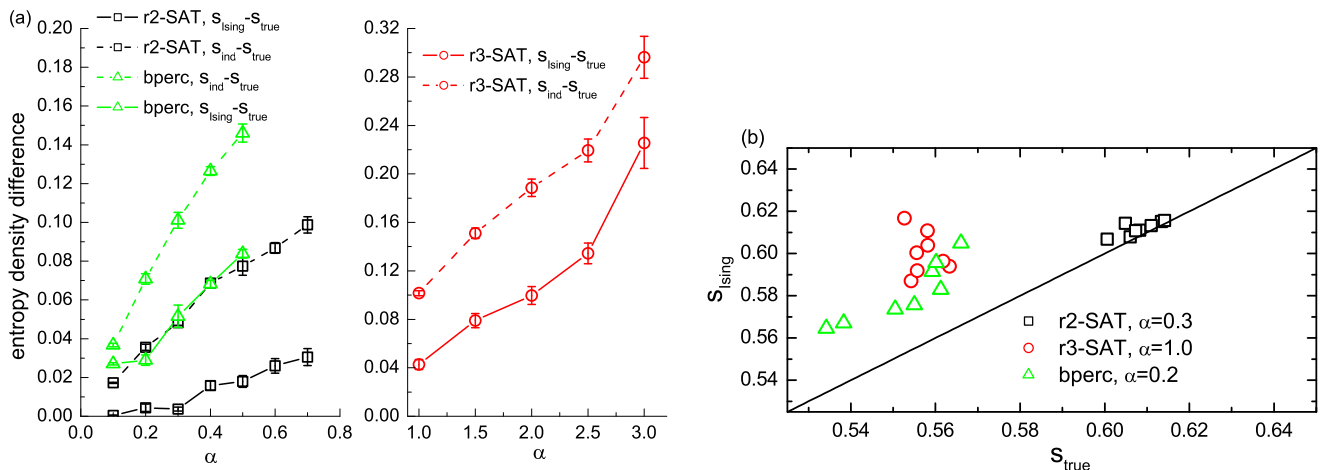


FIG. 1: (Color online) The quality of the pairwise and independent models versus constraint density  $\alpha$ . (a) Entropy density difference versus  $\alpha$ . The data points connected by dashed line are the differences between  $s_{\text{ind}}$  and  $s_{\text{true}}$ , while those connected by solid line are the differences  $s_{\text{Ising}} - s_{\text{true}}$ . The number of variables  $N = 100$  for random  $K$ -SAT (r2-SAT or r3-SAT) problem and 101 for binary perceptron (bperc).  $s_{\text{true}}$  is computed with the knowledge of the original model using belief propagation [23, 24]. Each point represents the average over eight random samples. (b) Scatter plot comparing  $s_{\text{Ising}}$  with  $s_{\text{true}}$ . The full line indicates equality.

higher-order correlations in its solution space or energy landscape. The different natures of these examples imply wide applications of our methodology to evaluate the entropy of an unknown model with only a limited number of samplings.

### A. Random $K$ -SAT problem

The random  $K$ -SAT problem is finding a solution (an assignment of  $N$  boolean variables) satisfying a random formula composed of logical AND of  $M$  constraints [25]. Each constraint is a logical OR function of  $K$  randomly chosen distinct variables (either directed or negated with equal probability). The constraint density  $\alpha = M/N$ . For  $K = 2$ , the threshold separating a SAT phase from an UNSAT phase was confirmed to be  $\alpha_s = 1$  below which the solution space is ergodic and a simple local search algorithm can easily identify a solution [25]. For  $K = 3$ , the estimated threshold  $\alpha_s \simeq 4.267$  below which the solution space exhibits richer structures [26]. The dynamical transition point locates at  $\alpha_d \simeq 3.86$  and separates the ergodic phase from non-ergodic phase. We use SEQSAT algorithm of Ref. [27] to first find a solution for a given  $\alpha$ , then  $10^8 N$  single variable flips are performed in the current solution space, after that we perform random walks in the current solution space to sample one solution every  $10^4$  steps. Each step involves  $N$  attempts to move from one solution to its adjacent one by single variable flip, i.e., a randomly chosen variable is flipped and if the new configuration is a solution, the flip is accepted with probability  $1/2$ ; otherwise the movement is rejected. We sample totally  $P = 10^5$  solutions to estimate the entropy. We choose  $\epsilon = 0.128$ ,  $\eta^{(1)} = 10^{-3}$  for random 2-SAT and  $\epsilon = 0.002$ ,  $\eta^{(1)} = 10^{-4}$  for random 3-SAT. Results are reported in Fig. 1. When  $\alpha$  is small, our method can predict the true entropy very well especially for  $K = 2$  which can be actually transformed into a pairwise Ising model. As  $\alpha$  increases, the difference between  $s_{\text{Ising}}$  and  $s_{\text{true}}$  [23] becomes large and this deviation is more obvious for  $K = 3$ , which manifests the presence of higher-order correlations in the solution space. At high  $\alpha$  (e.g.,  $\alpha = 3.0$  for  $K = 3$ ), the belief propagation Eq. (4) would yield multiple fixed points. This signals ergodicity breaking phenomenon in the energy landscape of the constructed Ising model or indicates that long range correlations develop in the original system [6], although our samplings are still confined in a single cluster of the original model, as a result, the predicted entropy becomes rather inaccurate compared with the true one computed under the original model.

### B. Binary perceptron

The binary perceptron with  $N$  binary weights connecting  $N$  input nodes to a single output node performs a random classification of  $\alpha N$  random binary patterns  $\{\xi_i^\mu\} (i = 1, \dots, N; \mu = 1, \dots, \alpha N)$ . The critical constraint

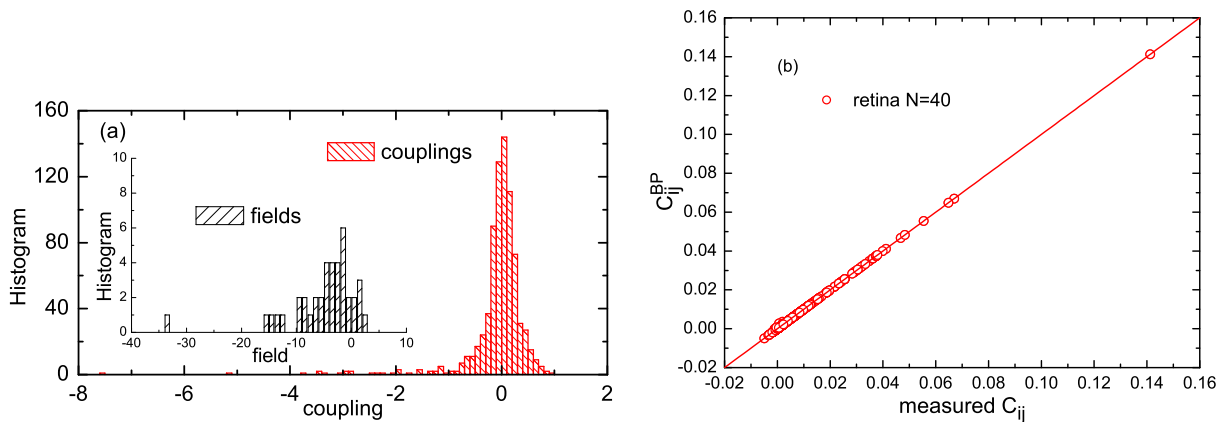


FIG. 2: (Color online) (a) Histograms of inferred couplings and fields (inset) for the retinal network with the number of neurons  $N = 40$  (data courtesy of Gasper Tkacik, Refs. [7, 8]). To infer the network, we choose  $\epsilon = 0.128$ ,  $\eta^{(1)} = 10^{-3}$ . The network is inferred at  $R_{\max} = 0.959$ . (b) Reconstructed  $C_{ij}^{\text{BP}}$  using belief propagation Eq. (6) versus the measured one. We only show the case  $i \neq j$  since  $C_{ii}^{\text{BP}} = 1 - (m_i^{\text{BP}})^2$ . The full line indicates equality.

TABLE I: Estimated entropy density  $s_{\text{BP}}$  for the inferred retinal network through belief propagation Eq. (4).  $q_0 = \frac{1}{N} \sum_i m_i^{\text{BP}} m_i$  where  $m_i^{\text{BP}}$  is computed from the fixed point of belief propagation Eq. (4). The self-overlap  $q_1 = \frac{1}{N} \sum_i m_i^2 \simeq 0.906828$ . The last column gives the probability of appearance for each fixed point during 1000 runs of belief propagation with the same inferred parameters.

$s_{\text{BP}}$	$q_0$	prob. app
0.09771	0.906816	0.089
0.1093	0.512411	0.075
0.1224	0.313566	0.066
0.1634	0.281124	0.400
0.1765	0.021960	0.354
0.1918	0.264979	0.016

density  $\alpha_s \simeq 0.83$  below which the solution space is non-empty [28]. Given an input pattern  $\xi^\mu$ , if the actual output  $o^\mu = \text{sgn} \left( \sum_{i=1}^N \sigma_i \xi_i^\mu \right)$  is equal to the desired output  $o_0^\mu$  assigned a value  $\pm 1$  with equal probabilities, the configuration  $\sigma$  learns this pattern. The solution space of the binary perceptron consists of all configurations learning  $\alpha N$  random patterns. Before sampling, we first learn  $\alpha N$  patterns using DWF algorithm of Ref. [29]. The sampling procedure is the same as that used for random  $K$ -SAT problems. In numerical simulations, we choose  $\epsilon = 0.001$ ,  $\eta^{(1)} = 10^{-4}$ . The deviation of estimated  $s_{\text{Ising}}$  from  $s_{\text{true}}$  [24] is plotted against  $\alpha$ . For small  $\alpha$ , our method can predict the true entropy well without the knowledge of the original model. The large deviation shown in Fig. 1 at high  $\alpha$  implies higher-order correlations start to dominate the solution space.

### C. Retinal network

A recording of the activity of 40 neurons in a salamander retina under natural movie stimuli could also be analyzed within the current setting. The total effective number of samplings  $P \simeq 7 \times 10^4$  [8]. Our estimated entropy density for the retinal network is  $s_{\text{BP}} \simeq 0.09771$  consistent with that obtained by Gasper Tkacik et.al [8] using Monte Carlo method which produces an estimate  $s_{\text{MC}} \simeq 0.09479$  but is rather time consuming for large  $N$ . Our result implies that the retina under the naturalistic movie stimuli stores  $e^{N s_{\text{BP}}} \simeq 50$  effective configurations. If we approximate the true entropy using that calculated by belief propagation (Eq. (3) and Eq. (4)) or Monte Carlo method, then the multi-information measuring the total amount of correlations in the network [30]  $I_{\text{BP}} = s_{\text{ind}} - s_{\text{BP}}$  or  $I_{\text{MC}} = s_{\text{ind}} - s_{\text{MC}}$  where  $s_{\text{ind}}$  is the independent entropy density. The result is that the difference between these two multi-information values  $I_{\text{MC}} - I_{\text{BP}} \simeq 0.00292$ . The histogram of inferred parameters is shown in Fig. 2 (a). Note that most of predicted couplings concentrate around zero value with a long tail of distribution for large negative couplings whose

weights are rather small. Most of the predicted fields are negative since most of the neurons are silent across the movie presentations. Using the same inferred parameters, we run belief propagation Eq. (4) 1000 times from different random initializations. Several fixed points are found and one of them is consistent with the previous result [8] (see Table I). These fixed points represent different metastable states and the entropy measures the capacity of neurons to convey information about the visual stimulus which contains high-order correlation structure. The visual information could be encoded by identity of the basin of attraction [19] and these predicted metastable states may code for specific stimulus features. Therefore, the information of the inputs to the retina can be stored in the couplings and fields which generate a free energy landscape with multiple metastable states for redundant error correction [19]. Future research on neuronal population coding needs to elucidate this point.

In Fig. 2 (b), we verify that the inferred pairwise Ising model reproduces the measured connected correlations with very good agreement. The reconstructed correlations  $\{C_{ij}^{\text{BP}}\}$  can be computed by the following message passing algorithm [21, 31]:

$$m_{i \rightarrow j} = \frac{e^{h_i} \prod_{l \in \partial i \setminus j} (1 + \hat{m}_{l \rightarrow i}) - e^{-h_i} \prod_{l \in \partial i \setminus j} (1 - \hat{m}_{l \rightarrow i})}{e^{h_i} \prod_{l \in \partial i \setminus j} (1 + \hat{m}_{l \rightarrow i}) + e^{-h_i} \prod_{l \in \partial i \setminus j} (1 - \hat{m}_{l \rightarrow i})} \quad (5a)$$

$$\hat{m}_{l \rightarrow i} = \tanh J_{li} m_{l \rightarrow i} \quad (5b)$$

$$g_{i \rightarrow j, k} = \delta_{ik} + \sum_{l \in \partial i \setminus j} \frac{1 - m_{l \rightarrow i}^2}{1 - (m_{l \rightarrow i} \tanh J_{li})^2} \tanh J_{li} g_{l \rightarrow i, k} \quad (5c)$$

where two kinds of messages,  $m_{i \rightarrow j}$  and  $g_{i \rightarrow j, k}$  are updated. Once both messages for each directed link in the network are converged, i.e., iteration of Eq. (5) reaches fixed point, we compute the predicted connected correlations  $\{C_{ij}^{\text{BP}}\}$  via

$$C_{ij}^{\text{BP}} = (\tilde{C}_{ij} - m_i m_j) g_{j \rightarrow i, j} + (1 - m_i^2) g_{i \rightarrow j, j} \quad (6a)$$

$$\tilde{C}_{ij} = \frac{\tanh J_{ij} + m_{i \rightarrow j} m_{j \rightarrow i}}{1 + \tanh J_{ij} m_{i \rightarrow j} m_{j \rightarrow i}} \quad (6b)$$

where the Ising model is known and all messages needed to compute  $C_{ij}^{\text{BP}}$  including  $m_i$  and  $m_j$  are read from the fixed point. This message passing strategy to evaluate the correlations is very fast and takes tens of iterations to converge. Remarkably, the estimated magnetizations and correlations fit those measured very well. However, using Monte Carlo samplings to reconstruct the correlations, we failed to reproduce those measured. For example, after sufficient thermalization, the configuration is sampled every  $10^4$  Monte Carlo sweeps, then the correlations are computed with  $10^4$  sampled configurations. The obtained root mean square error is about 0.23. Possible reason is, the reconstructed Ising model by SusProp already develops multiple states (different fixed points of belief propagation Eq. (4)), therefore, at temperature  $T = 1.0$  and  $N = 40$ , as observed in our simulations, Monte Carlo samplings can have transitions between different states yielding the average energy density of sampled configurations  $\bar{e} \simeq -3.7119$  with fluctuation of order 0.0724 while the state reproducing the measured correlations in Fig. 2 (b) has typical energy density  $-3.62954$  but smallest entropy density  $s_{\text{BP}} \simeq 0.09771$  of all observed states. Actually, in this case, the correlation computed by Monte Carlo samplings corresponds to the average over different states while the measured data comes from one state of the reconstructed Ising model.

#### D. Convergence patterns and entropy density difference versus $P$

There exist three kinds of convergence patterns for different iterations of SusProp rules. One is the convergence case shown by an example of random 2-SAT with  $\alpha = 0.7$ ; the second type is the convergence fraction  $R$  first increases then decreases (see in Fig. 3 an example of binary perceptron with  $\alpha = 0.5$ ); the last type is  $R$  reaches a plateau with small fluctuations shown by an example of retina.

In Fig. 4(a), the influence of the number of samplings  $P$  on the estimation of entropy from the finite samplings is shown. It seems that the entropy density difference decreases as  $P$  becomes small. Note that we construct the pairwise Ising model based on the samplings from the ground state (zero energy for these three constraint satisfaction problems) and the underlying graphical model (e.g., r3-SAT or bperc) may not be a pairwise Ising model. Our samplings are always confined in a single solution cluster and the quality may depend on the fine structure of the solution space [32–34]. This case is different from studies on the reconstruction of Sherrington-Kirkpatrick model at high temperatures [20]. In our current setting, when the sampling number  $P$  decreases, the collected data seems to have more correlations (this may be induced by the statistical errors) and the SusProp turns out to be not converged any more (e.g., in the case of r2-SAT with  $\alpha = 0.3$ ), which can be justified from the Fig. 4(b) that the inferred

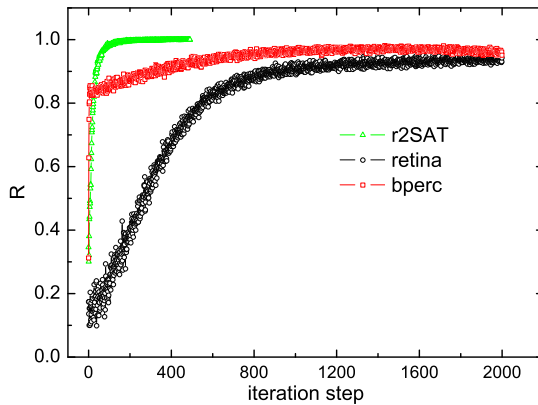


FIG. 3: (Color online) Convergence patterns possibly appearing in the iteration of SusProp update rules.

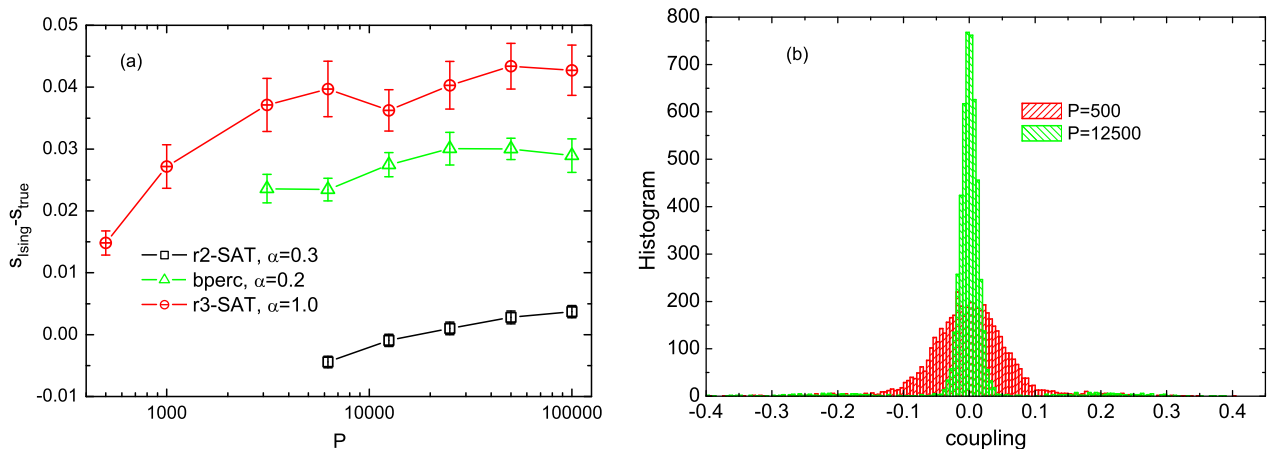


FIG. 4: (Color online) (a) Entropy density difference versus  $P$ . The error bar shows the fluctuation across eight random samples. (b) The distribution of inferred couplings for r3-SAT with  $\alpha = 1.0$  and  $N = 100$ . Two results for  $P = 500$  and  $P = 12500$  are shown.

coupling distribution becomes broader with decreasing  $P$  and thus the estimated entropy should take smaller values. As observed in Fig. 4(b), once  $P$  decreases down to some value, the estimated entropy value would underestimate the true one computed with the knowledge of the original model. On the other hand, given small  $P$ , the computed magnetizations and correlations would have large statistical errors and may not correctly reflect the correlations in the sampled solution cluster. Safely, we select  $P = 10^5$  to reduce the statistical error for calculating the magnetizations and correlations.

#### IV. CONCLUSION

In this work, we address the important problem of counting the total number of solutions (configurations) based on a limited number of sampled solutions (configurations). We formulate the solution (configuration) counting problem within the framework of inverse Ising problem, and this idea is tested on both diluted models and fully-connected models, as well as on real neural data. In the first case, we do not know a priori the underlying graphical models and try to construct a disordered Ising model from the collected data to evaluate the entropy of those unknown models. Note that the sampled solutions come from the zero energy ground state (single solution cluster) and the number is limited to  $P$  but the size of that sampled cluster is evaluated. To this end, the pairwise model improves substantially the independent model (see Fig. 1(a)). When the constraint density is small then the pairwise correlation dominates the solution space, the estimated entropy gets very close to the true one estimated with the knowledge of the original model. Another interesting point to be demonstrated in our further work is, for small  $N$ , one can compute the magnetizations and correlations through exact enumeration and further the real entropy value. The

result of Boltzmann learning algorithm [11] and Monte Carlo simulation [8] (using a large enough amount of Monte Carlo samplings) should provide an upper bound on the true entropy. Instead, using the approximate method we proposed, whether the obtained result provides a bound should be checked for small size system or proved in the limit of large  $N$ , provided that the magnetizations and correlations are less noisy. In the second case, the susceptibility propagation is applied to infer the retinal network and belief propagation is used to reproduce the entropy computed by Monte Carlo method. This message passing scheme is very fast and efficient especially for large network and the observed multiple fixed points predict other metastable states in the inferred retinal network. These metastable states may have intimate relation with the neuronal population coding [19]. Extensions to the neuronal interaction network organized in a hierarchical and modular manner would be very interesting [35, 36]. Our presented framework constructs a statistical mechanics description of the system directly from either artificial data or real data, and has the potential to describe biological networks more generally and estimate the size of the solution space in various contexts especially when pairwise correlation dominates the system.

### Acknowledgments

We thank Gasper Tkacik for providing us multielectrode recordings of the salamander retina. The improvement of the manuscript benefited from comments and suggestions of anonymous referees. The present work was partially supported by the NSFC Grant 10834014 and the 973-Program Grant 2007CB935903 and HKUST 605010.

- 
- [1] L. Valiant, *Theoretical Computer Sciences* **8**, 189 (1979).
  - [2] D. Roth, *Artificial Intelligence* **82**, 273 (1996).
  - [3] C. P. Gomes, J. Hoffmann, A. Sabharwal, and B. Selman, in *Proc. of IJCAI-07* (Hyderabad, India, 2007), pp. 2293–2299.
  - [4] L. Kroc, A. Sabharwal, and B. Selman, in *Proc. of CPAIOR-08* (Paris, France, 2008), pp. 127–141.
  - [5] A. Favier, S. de Givry, and P. Jégou, in *Proc. of CP-09* (Lisbon, Portugal, 2009), pp. 335–343.
  - [6] J. Bento and A. Montanari, in *Advances in Neural Information Processing Systems 22*, edited by Y. Bengio, D. Schuurmans, J. Lafferty, C. K. I. Williams, and A. Culotta (2009), pp. 1303–1311.
  - [7] E. Schneidman, M. J. Berry, R. Segev, and W. Bialek, *Nature* **440**, 1007 (2006).
  - [8] G. Tkacik, E. Schneidman, M. J. Berry, and W. Bialek (2009), e-print arXiv:0912.5409.
  - [9] S. Cocco and R. Monasson, *Phys. Rev. Lett* **106**, 090601 (2011).
  - [10] J. H. Macke, M. Opper, and M. Bethge, *Phys. Rev. Lett* **106**, 208102 (2011).
  - [11] D. H. Ackley, G. E. Hinton, and T. J. Sejnowski, *Cognitive Science* **9**, 147 (1985).
  - [12] M. Mézard and T. Mora, *J. Physiology Paris* **103**, 107 (2009).
  - [13] Y. Roudi, J. Tyrcha, and J. Hertz, *Phys. Rev. E* **79**, 051915 (2009).
  - [14] V. Sessak and R. Monasson, *J. Phys. A* **42**, 055001 (2009).
  - [15] M. Weigt, R. A. White, H. Szurmant, J. A. Hoch, and T. Hwa, *Proc. Natl. Acad. Sci. USA* **106**, 67 (2009).
  - [16] S. Cocco, S. Leibler, and R. Monasson, *Proc. Natl. Acad. Sci. USA* **106**, 14058 (2009).
  - [17] T. Mora, A. M. Walczak, W. Bialek, and J. C. G. Callan, *Proc. Natl. Acad. Sci. USA* **107**, 5405 (2010).
  - [18] A. Tang, D. Jackson, J. Hobbs, W. Chen, J. L. Smith, H. Patel, A. Prieto, D. Petrusca, M. I. Grivich, A. Sher, et al., *J. Neurosci* **28**, 505 (2008).
  - [19] G. Tkacik, J. S. Prentice, V. Balasubramanian, and E. Schneidman, *Proc. Natl. Acad. Sci. USA* **107**, 14419 (2010).
  - [20] E. Marinari and V. V. Kerrebroeck, *J. Stat. Mech.: Theory Exp* **P02008** (2010).
  - [21] H. Huang, *Phys. Rev. E* **82**, 056111 (2010).
  - [22] M. Mézard and G. Parisi, *Eur. Phys. J. B* **20**, 217 (2001).
  - [23] K. Li, H. Ma, and H. Zhou, *Phys. Rev. E* **79**, 031102 (2009).
  - [24] A. Braunstein and R. Zecchina, *Phys. Rev. Lett* **96**, 030201 (2006).
  - [25] R. Monasson and R. Zecchina, *Phys. Rev. Lett* **76**, 3881 (1996).
  - [26] F. Krzakala, A. Montanari, F. Ricci-Tersenghi, G. Semerjian, and L. Zdeborova, *Proc. Natl. Acad. Sci. USA* **104**, 10318 (2007).
  - [27] H. Zhou, *Eur. Phys. J. B* **73**, 617 (2010).
  - [28] W. Krauth and M. Mézard, *J. Phys. (France)* **50**, 3057 (1989).
  - [29] H. Huang and H. Zhou, *J. Stat. Mech.: Theory Exp* **P08014** (2010).
  - [30] E. Schneidman, S. Still, M. J. Berry, and W. Bialek, *Phys. Rev. Lett* **91**, 238701 (2003).
  - [31] S. Higuchi and M. Mézard, *J. Phys.: Conf. Ser* **233**, 012003 (2010).
  - [32] H. Zhou and H. Ma, *Phys. Rev. E* **80**, 066108 (2009).
  - [33] A. Mann and A. K. Hartmann, *Phys. Rev. E* **82**, 056702 (2010).
  - [34] H. Huang and H. Zhou, *Europhys. Lett* **96**, 58003 (2011).
  - [35] I. E. Ohiorhenuan, F. Mechler, K. P. Purpura, A. M. Schmid, Q. Hu, and J. D. Victor, *Nature* **466**, 617 (2010).

[36] E. Ganmor, R. Segev, and E. Schneidman, Proc. Natl. Acad. Sci. USA **108**, 9679 (2011).